

SoftCharge: Software Defined Multi-Device Wireless Charging Over Large Surfaces

Kai Li¹, Student Member, IEEE, Ufuk Muncuk¹, Student Member, IEEE, M. Yousof Naderi, Member, IEEE, and Kaushik Roy Chowdhury, Senior Member, IEEE

Abstract—This paper proposes a method for converting a large existing surface into a programmable wireless charger, capable of distributing energy efficiently at multiple locations on demand and charge different types of devices. The key innovation here is to combine magnetic resonance-based energy transfer with the so called concept of ‘energy hopping’ across wireless inter-connected coils, where the magnetic fields are carefully shaped on the fly. The overall framework, called SoftCharge, has three components: (i) energy tiles (ETs), which are individual programmable coil units that can be attached underneath an existing table with AC mains supply only to the master tile, (ii) energy shaping algorithm executed by the master tile, that shapes the flow of energy over tiles through real-time impedance adjustment combined with selective power blocking, creating optimal energy paths to specific tiles where a device needs to be charged, and (iii) a resonance sensing architecture design and method executed in each given tile that detects the type of device to be charged and its location without any direct feedback. We build a prototype of energy tiles and provide experimental results on SoftCharge charging multiple COTS devices like mobile phones, laptops, tablets, and drones, resulting in a maximum charging rate of 23 W up-to 20 cm over a large surface.

Index Terms—Wireless power transfer, magnetic resonant coupling, energy hopping, magneto-inductive wave.

I. INTRODUCTION

SINCE Nikola Tesla’s first demonstration of wireless power transfer a century ago [1], harnessing the energy contained in magnetic fields for wireless power transfer is seeing increasing interest. There are mature standardization efforts that have evolved around Wireless Power Consortium (WPC) supported Qi [2] that uses both magnetic induction and resonance, and the AirFuel Alliance that uses magnetic resonance [3]. These technologies power many consumer devices, such as phones and laptops [4], cars [5], [6] and drones [7], [8]. Yet, the state-of-the-art solutions address point-charging needs for a single device at a time, with a localized area of action. We propose a software defined magnetic resonant charging architecture, called SoftCharge, which can potentially transform an existing large surface into a multi-device charger.

Manuscript received October 5, 2019; revised January 18, 2020 and February 6, 2020; accepted February 8, 2020. Date of publication February 13, 2020; date of current version March 12, 2020. This article was recommended by Guest Editor S. Abadal. (Corresponding author: Kai Li.)

The authors are with the Department of Electrical and Computer Engineering, Northeastern University, Boston, MA 02115 USA (e-mail: likai2@coe.neu.edu).

Color versions of one or more of the figures in this article are available online at <https://ieeexplore.ieee.org>.

Digital Object Identifier 10.1109/JETCAS.2020.2973814

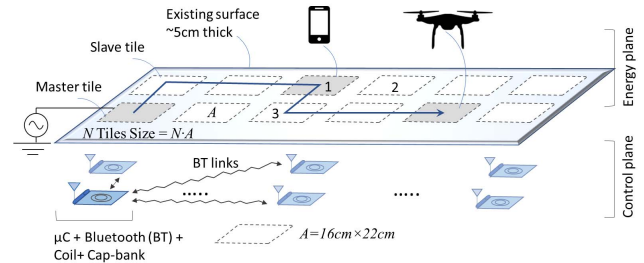


Fig. 1. SoftCharge energy tiles attach on the under-side of a given surface. Multiple number and types of devices, from UAVs to phones, can be charged through energy-on-demand device localization and adaptive energy hopping across tiles.

A. Using Magnetic Field for Energy Transfer

We envisage a scenario shown in Fig. 1, with a large planar surface of a suitable non-metallic material (wood, glass, plastic). Each tile (without extra PCB digital controller unit) has dimensions of $A = 16\text{cm} \times 22\text{cm}$. The overall size of whole system with N tiles is approximately $N \cdot A$. Multiple object types, such as phones, laptops, drones, wearables, among others, may either be placed on the surface all at once or hover in close proximity for charging. We next discuss our motivation for designing a new architecture for wireless power transfer for such a scenario.

Qi-based magnetic induction permits only few mm of alignment mismatch between the transmitter-receiver coils. Our work considers the Qi-based system in the magnetic inductive mode, since most of the current Qi products work in this mode [9]. Moreover, to cover a large surface, we need hundreds of coils, each with its own power management circuit per coil. This dramatically increases the cost and complexity. Moreover, this requires specialized power sockets to ensure hundreds of coils are continuously sensing (each typically consumes $1/3\text{W}$ in this state [10]), even when there are no devices to be charged. Thus today’s commercial Qi solutions only offer at most three-coil charging.

Different approaches towards creating wireless power transfer surfaces exist. The metasurface based wireless charging system in [11], [12] operate at a high frequency in the range hundreds of MHz or GHz. While theoretically feasible, there are practical issues concerning availability of efficient receivers for powering COTS devices like phone, laptop or UAV in these frequencies. A capacitive coupling based metasurface charging system [13] provides a novel approach towards multi-device charging, although it poses a risk towards

other conductive materials, such as human tissues, compared to inductive coupling methods.

Using magnetic resonance overcomes the requirement of direct contact, although each coil now must have its own separate power amplifier, explicit receiver-generated feedback, phase adjustment circuits and inter-coil synchronization. A seminal advancement here is using beamforming to constructively combine magnetic field energy supplied by multiple coils [14]. However, this work does not distinguish and regulate power transfer for different types of objects. Additionally, the sensing in magnetic resonance is more complex and thus incurs higher cost than the inductive-backscatter method used in Qi. Finally, there are no FCC approved products that allow magnetic resonance over large distances owing to the challenges in containing the interference range.

B. Proposed Solution: SoftCharge

As shown in Fig. 1, SoftCharge uses magnetic resonance but limits the range of a given coil by placing a large number of them in two dimensions. A single coil, a wireless network interface connected to a low-power micro-controller, and a dual capacitor bank together compose a so called *energy tile*. Only the *master* tile has its own power amplifier and connected to an AC socket, while all other *slave* tiles have no connection to AC power. SoftCharge tiles attach to the underside of the table surface, and form a wireless mesh network control plane using OpenThread [15]. This allows the tiles to perform coordinated sensing and deliver energy within the energy plane in a cooperative manner anywhere around the table surface..

The software defined framework that executes in the master tile allows SoftCharge to localize the object to the closest tile, detect the type of object, and then deliver energy to that specific tile (or multiple tiles in case of more than one object) through the concept of *energy hopping* over tiles. Since all slave tiles are passive in the sense that they lack power amplifiers, this modular design and energy distribution method is easily extensible to any surface area. The master tile executes an optimization algorithm that decides the intermediate tiles (for example, tile 3 in Fig. 1) that should participate in the energy hopping path shown by the arrow. The energy path must connect the tiles over which the charging objects exist. The optimization also identifies the tiles (for example, tile 2) that should block all energy flow over it. These roles are communicated over the control plane by the master to all the slave tiles, which set their impedance in accordance with the assigned roles.

C. Summary of Contributions

This paper makes the following hardware and software contributions:

- We introduce the concept of software-defined wireless charging over re-configurable, networked units called energy tiles.
- We propose an out-of-band sensing method that uses a multi-coil system to identify the presence of objects that are placed on or hover above the surface. The approach

does not require involvement of the receiver coil and incurs mW-scale power consumption.

- We formulate and solve the optimization problem that identifies tiles that must be energy recipients, energy relays and those that must block energy over them.
- We develop the theory of energy hopping over a 2-D plane with flexible paths that by adjusting coil-impedance through using software directives. This allows any point-to-point energy delivery with only a single active source of power.
- We present implementation results for wireless charging of a phone, laptop, and UAV, through measurements at realistic locations of a library, cafe, and home that have surfaces of 4 cm thickness with different areas and compositions.

The rest of the paper is organized as follows. Sec. II surveys the related work. A novel object sensing approach is described in Sec. III. We derive the theory for directing energy flow across a 2-D grid of tiles placed under a surface in Sec. IV while Sec. V formulates an optimization problem to selectively assign roles to these tiles. Sec. VI gives the design of optimizing the receiver through a multi-coil relay arrangement. Sec. VII and Sec. VIII give the system implementation details and the stage-wise experimental results from a lab test setup. Finally, we demonstrate SoftCharge for specific applications in Sec. IX and conclude the paper in Sec. X.

II. RELATED WORK

As discussed earlier, magnetic induction-based methods, such as Qi, are effective at less than 5mm gap between the transmitter-receiver coils [16]. In a different approach, wireless power transfer using strongly coupled magnetic resonance can potentially overcome these distance limitations. Prior research in [17] has shown that such coupling can deliver power over 2m distance with more than 40% efficiency. The seminal work on Magnetic MIMO [14], [18] attempts to increase wireless power transfer distance by leveraging the principle of MIMO-beamforming commonly used in classical RF communication. The implemented testbed uses six coils, each connected to its own power amplifier. SoftCharge attempts to reduce the number of power amplifiers down to one, irrespective of the surface dimension. Magnetic MIMO reports about 10s latency between an object being placed, and its successful detection at the end of the sensing round. Furthermore, it necessarily requires a receiver coil to ensure sufficient mutual coupling with the transmitter coil, and thus accurate detection. SoftCharge, on the other hand, reduces the sensing time to few ms, and does not require the involvement of the receiver coil during sensing.

A potential solution to reduce the number of costly amplifiers (the single most expensive part of the design) relies on the so called *domino coil* concept [19]. This concept is based on Tesla's Resonator, where each passive resonant coil acts as a relay and extends the reach of the magnetic field to a longer distance, for example, lighting a 14W lamp 3m away from the source coil [20]. While SoftCharge also uses the concept of domino coils, prior works are limited

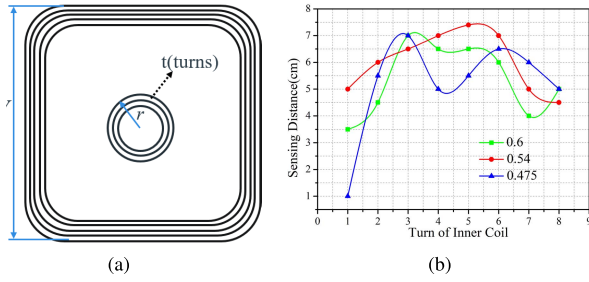


Fig. 2. (a) Sensing coil layout and (b) the relationship between sensing distance and coil parameters.

to placing all the relay coils at an orientation perpendicular to a horizontal plane. Thus, existing theoretical formulations governing energy propagation in vertical coils do not apply to our proposed surfacing charging scenario.

Planar coil energy relaying described in [21], [22] comes closest to SoftCharge. The main differences with our work are as follows: (i) These works transfer mW power to the receiver and mainly validate the theory of energy hopping. SoftCharge delivers four orders of magnitude more power and demonstrates true wireless charging. (ii) They suffer from the problem of undesirable nullification at specific locations caused by reflected waves, which does not allow charging at any random coil. SoftCharge solves this problem through software-based impedance optimization that eliminate the reflected wave. (iii) SoftCharge extends the energy hopping theory from 1-D to 2-D, and thus enables a practical surface charging paradigm. (iv) While these works only propagate energy along a straight chain, SoftCharge can flexibly create paths with turns, as shown in Fig. 1.

Finally, fine-grained energy delivery also requires accurate object sensing. Wireless localization solutions based on reflected RF signals from Bluetooth, ZigBee, RFID, Wi-Fi, UWB radios [23], backscatter [24] require a second (receiver) device and/or additional signal reflectors. It is also necessary to receive feedback from the receiver to estimate the channel state at the transmitter side. State of the art near-field magnetic induction based sensing solutions, have the same shortfalls as energy transfer. For example, inductive sensing in Qi is limited in distance to few mm and also requires perfect alignment between coils [16]. Finally, other low-cost sensing solutions such as resistive sensing [25] and capacitive coupling [26] are not capable of sensing materials other than non or low-conductive objects.

III. LOW-POWER RESONANCE SENSING

In this section, we present a novel sensing technique using a nested coil arrangement shown in Fig. 2a. The main idea here is to use two coils, with AC voltage applied to the inner coil and variations in the induced voltage are then measured across the load in the outer coil. Our design accounts for the tradeoff in sensing coverage with power consumption. This is because larger coils cover more of the surface, but incur higher power consumption. Smaller coils consume less power, but many more of them must be used for similar sensing coverage. The sensing goal is to detect an object and its type upto a range of several *cm* above the surface.

Our sensing method uses an AC voltage signal applied to the inner coil in the KHz range (as is also used in Qi). There are two reasons for this: First, the detecting signal variations in the passive outer coil is much simpler, as compared to variations in a MHz-band signal. Our preliminary results indicated 65% accuracy improvement using the similar coil dimensions with 16-bit ADCs as a result of this design choice. Another reason for using KHz range sensing is to overcome the skin effect. In this dual-coil arrangement, the outer coil acts a resonator relay, that sets up a magnetic flux generated by the induced voltage in it, with very little loss compared to directly applying the AC signal to it. When a target object (such as cell phone, laptop, tablet, and UAV in our case) comes close to the surface, the induced voltage in the outer coil changes. These objects, owing to the different levels of component conductive materials, uniquely alter the induced voltage. This change, $|\Delta V|$, is measured at the outer coil, and then compared to the threshold $|\Delta V_{thre}|$ to confirm the type or location of the devices. At this stage, the signal is noisy and depends on multiple properties of the object, such as size, shape, materials, magnetic permeability, electrical conductivity. It also depends on the overlapping area and the distance between the object and the outer coil.

Using the notations for inner(in) and outer(out) coils, formally, the circuit variables can be computed via standard approaches given by,

$$V_{in} = I_{in}(j\omega_s L_{in} + \frac{1}{j\omega_s C_{in}} + Z_{in}) + j\omega_s M_{in,out} I_{out} \quad (1)$$

$$I_{out}(j\omega_s L_{out} + \frac{1}{j\omega_s C_{out}} + Z_{out}) + j\omega_s M_{in,out} I_{in} = 0 \quad (2)$$

where V_{in} , I_{in} , I_{out} , L_{in} , L_{out} , C_{in} , C_{out} , Z_{in} , Z_{out} are source voltage, current, inductance, capacitance, impedance of inner and outer coils, respectively. $M_{in,out}$ gives the mutual inductance between the inner and outer coils. Here ω_s with subscript s represents the angular frequency used for sensing, and ω without subscript s represents the wireless charging angular frequency in the rest of the manuscript. Since both coils are at the resonance state, the terms $j\omega_s L$ and $\frac{1}{j\omega_s C}$ cancel each other. The voltage of outer coil, when there is no object to be detected, is:

$$V_{out} = j\omega_s M_{in,out} I_{in} \quad (3)$$

$$V_{out} = -I_{out} Z_{out} \quad (4)$$

Once a device is placed in the coverage range of the outer coil, the complex impedance Z_{out} changes to Z'_{out} without changing the current I_{out} , since the input power and output voltages are not changed with or without nearby objects. Thus, the voltage change on the outer coil can be calculated as

$$|\Delta V| = |I_{out}(Z'_{out} - Z_{out})| \quad (5)$$

Fig. 2a depicts the layout of our sensing coil, where W is the width of outer coil, r is the radius of inner coil, and t gives the number of turns for the inner coil. The layout and material of sensing coil impact the performance of sensing, both in terms of sensitivity and range. We consider the sensing range as the threshold point at which the induced voltage $|\Delta V|$ falls

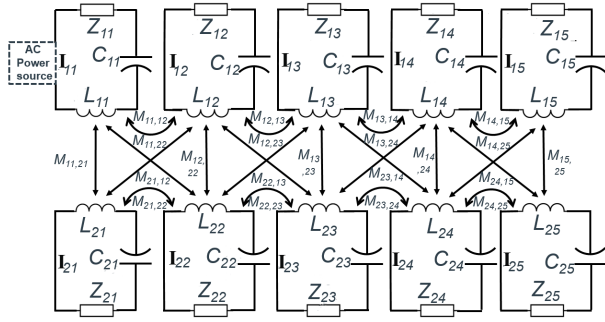


Fig. 3. Circuit Diagram of tiles array.

below 50 mV. Fig. 2b depicts the results of sensing an iPhone 8 with different turns and ratios between outer and inner coils, marked as 0.6, 0.54, 0.475. We experimentally observe that the number of turns for inner coil directly impacts the average sensing distance, and this value is up to 7 cm for our phone sensing results. The three lines in the plot correspond to different $\kappa = \frac{2r}{W}$ ratios. From these measurements, we select 6 turns for the inner coil as it shows a peak for multiple κ values. Inner coil with 3 turns is also an acceptable value, although the instantaneous variations are much higher than the more stable results at 6 turns.

IV. THEORETICAL FRAMEWORK FOR ENERGY HOPPING

In this section, we first present our analytical energy model for a network of multiple energy tiles placed over a 2-D surface. To this end, we model the energy flow by selecting the capacitors connected to a given coil, and through this process, we also adjust the resonance between coils. Prior works have used 1-D energy hopping by using resistors to eliminate Magneto-inductive (MI) wave reflection [21], [27]. SoftCharge makes several novel contributions in the process of extending energy hopping to 2-D as follows. (i) In the resistor-based approach used in 1-D hopping, the resistive element acts as a load and converts electrical energy to heat. Thus it does not support practical wireless charging applications requiring high power levels. SoftCharge is the first attempt to analyze capacitance-based energy hopping over a surface. A capacitor acts as a passive component; in the ideal case, its zero resistance does not consume any power. (ii) We model two important factors in the power distribution across 2-D placement of energy tiles that is not covered in prior work: energy cancellation due to reflection of power between tiles, and power loss incurred during over-the-air hopping over multiple tiles. Then we present our capacitance-based impedance optimization method that maximizes the received power delivered to the sensed devices, while minimizing both the total transmitted power and power loss.

A. 2-D Impedance Modeling

Fig. 3 shows a set of energy tiles placed under a given surface.

Here, in the ideal case with infinite number of energy tiles, each energy tile has strong mutual coupling with its four neighboring tiles along both vertical and horizontal sides. For

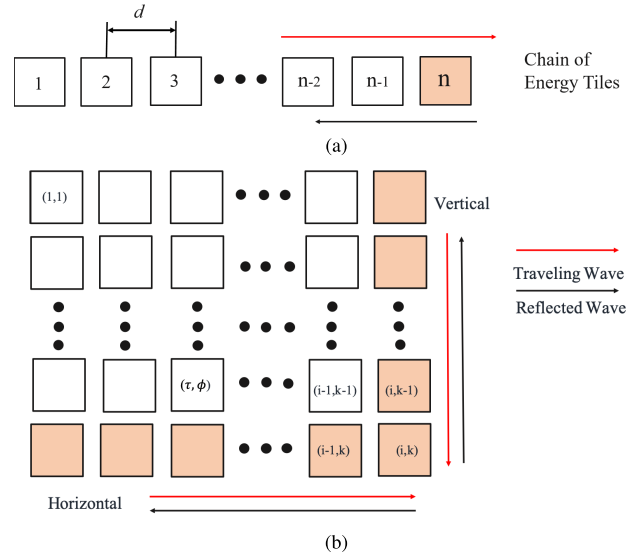


Fig. 4. Magneto-inductive wave transmission and reflection in 1-D (a) and 2-D (b) surface.

the practical case with limited number of tiles, limited rows or columns, some tiles have less than four neighbouring tiles. The theory and the following equations still work for such cases, but the missing tiles contribute 0 mutual coupling. The coupling between any pair of diagonal tiles is close to zero due to weak magnetic field overlap among them. L , C , Z , and \mathbf{I} denote the generic inductance, capacitance, impedance and current of each tile in the 2-D surface with i row k column and terminated by the last tile (i,k) . While individual mutual coupling are identified through different subscripts, we simplify the notation to a constant M in the rest of the paper, as all tiles are identical.

Π represents four mutual inductance with current between a generic tile and its two vertical neighbors and two horizontal neighbors. The master tile has two vertical neighbors and one horizontal neighbour, giving mutual inductance as $M_{11,12}$ and $M_{11,21}$, respectively.

The master tile in Fig. 3 connected to an AC power source can be defined by the following electrical parameters:

$$\mathbf{V}_s = \mathbf{I}_{11}(j\omega L_{11} + \frac{1}{j\omega C_{11}} + Z_{11}) + j\omega M_{11,21}\mathbf{I}_{21} + j\omega M_{11,12}\mathbf{I}_{12} \quad (6)$$

For the rest of the tiles (τ, ϕ) in the 2-D surface, $1 \leq \tau \leq i$ and $1 \leq \phi \leq k$, we have:

$$\mathbf{I}_{\tau\phi}(j\omega L_{\tau\phi} + \frac{1}{j\omega C_{\tau\phi}} + Z_{\tau\phi}) + j\omega \Pi_{\tau\phi} = 0 \quad (7)$$

where Π at tile (τ, ϕ) has:

$$\Pi = M_{\tau\phi, \tau-1\phi}\mathbf{I}_{\tau-1\phi} + M_{\tau\phi, \tau\phi-1}\mathbf{I}_{\tau\phi-1} + M_{\tau\phi, \tau\phi+1}\mathbf{I}_{\tau\phi+1} + M_{\tau\phi, \tau+1\phi}\mathbf{I}_{\tau+1\phi} \quad (8)$$

B. MI Wave Reflections and Energy Cancellation

In both the cases involving a chain of finite resonating tiles shown in Fig. 4a or over a 2-D surface Fig. 4b, we have two types of MI waves: The first is a forward wave that is generated

by source and travels through energy hopping towards the last coil. The second is the reflected wave that is setup at the last coil in the chain [27] and travels back along the opposite direction of the forward wave. In a 2-D surface composed of a grid $i \times k$ energy tiles, considering a single source and terminated by tile (i,k) , we note that reflected waves from the termination impacts the current distribution of any tile of the 2-D surface.

The key challenge for optimizing power delivery is to avoid destructive interference of the forward/reflected waves. In a chain of energy tiles shown in Fig. 4a, the current traveling along the tile chain in each tile n can be expressed as follows [27]–[29]:

$$\mathbf{I}_n = I e^{-j\gamma n d} \quad (9)$$

where, I is the amplitude of the current along the chain of tiles, d is the fixed distance between neighboring tiles, γ is the propagation constant given as $\frac{2\pi}{\lambda}$, where λ is resonating AC power source wavelength. The circulating currents in the last three coils of the chain with the last (n^{th}) as the termination can now be expressed as [21], [27]:

$$Z_n \mathbf{I}_n + H \mathbf{I}_{n-1} = 0 \quad (10)$$

$$Z_{n-1} \mathbf{I}_{n-1} + H(\mathbf{I}_n + \mathbf{I}_{n-2}) = 0 \quad (11)$$

Here, $H = j\omega M$, and we further simplify $Z_n = Z_{n-1} = Z$ as the impedance of the tiles. We keep the same notation in the analysis for the 2-D surface in section IV-A. The reflection coefficient can be defined as $\rho_T = \frac{R}{I}$ [21], where the forward wave arrives at the last tile, located at the n^{th} position in the chain with current amplitude of I and the reflected wave amplitude from it is R . Then the reflection ratio at other points in the chain before the termination is defined as [21]:

$$\begin{aligned} \rho_m &= \frac{R e^{-j(m-1)\gamma d}}{I e^{j(m-1)\gamma d}} = \rho_T e^{-2j(m-1)\gamma d} \\ \rho_T &= \frac{H^2 - (Z + H e^{j\gamma d})Z}{(Z + H e^{-j\gamma d})Z - H^2} \end{aligned} \quad (12)$$

where m is the number of tiles before the termination tile, m is used in 2-D surface for each row or column with same methodology in the chain of energy tiles. Since the reflection occurs from the termination tile, the subscript index order of reflection ratio is opposite to the subscript of the current distribution in (9). Substituting the reflection ratio in (10) and (11) for the last three tiles we get for the case of $m = 2$:

$$\mathbf{I}_{n-1} = I + R = I(1 + \rho_T) \quad (13)$$

$$\mathbf{I}_{n-2} = I(e^{j\gamma d} + \rho_T e^{-j\gamma d}) \quad (14)$$

and the current distribution of termination is obtained as:

$$\mathbf{I}_n = -\frac{Z}{H} I(1 + \rho_T) - I(e^{j\gamma d} + \rho_T e^{-j\gamma d}) \quad (15)$$

For each intermediate resonating coil with high quality factor and power transfer efficiency, the coil's impedance Z is very small and is approximated as zero [30], [31]. Then $\rho_T = -1$ as Z does not change from (12). Thus, the current amplitude in the coil at $(n-1)^{\text{th}}$ is equal to zero and the amplitude of current at n^{th} and $(n-2)^{\text{th}}$ tile are same. The power at $(n-1)^{\text{th}}$ is zero due to the interference between

transmitted and reflected waves as $(n-2)^{\text{th}}$ tile is considered as the new termination tile for the chain with $n-2$ tiles. Using the same approach used in an n tile chain, we get the current distribution of each tile, with details given in section V-A.

As mentioned in section IV-A, there is mutual coupling between two vertical and two horizontal tiles. Thus in a 2-D surface, we define the vertical reflection coefficient before the termination column k as:

$$\begin{aligned} \rho_m^v &= \rho_T^v e^{-2j(m-1)\gamma d} \\ &= \frac{H^2 - (Z + H e^{j\gamma d})Z}{(Z + H e^{-j\gamma d})Z - H^2} e^{-2j(m-1)\gamma d} \end{aligned} \quad (16)$$

Similarly, the horizontal reflection coefficient for tiles before the termination row i is:

$$\begin{aligned} \rho_m^h &= \rho_T^h e^{-2j(m-1)\gamma d} \\ &= \frac{H^2 - (Z + H e^{j\gamma d})Z}{(Z + H e^{-j\gamma d})Z - H^2} e^{-2j(m-1)\gamma d} \end{aligned} \quad (17)$$

where $\rho_T^h, \rho_T^v = \rho_T$. The net reflection at each tile before the termination in the 2-D surface consists of both vertical and horizontal reflected waves. This is calculated as:

$$\begin{aligned} \rho_m^{v,h} &= \rho_T^{v,h} e^{-2j(m-1)\gamma d} = (\rho_T^v + \rho_T^h) e^{-2j(m-1)\gamma d} \\ &= \frac{H^2 - (Z + H e^{j\gamma d})Z}{(Z + H e^{-j\gamma d})Z - H^2} e^{-2j(m-1)\gamma d} \\ &\quad + \frac{H^2 - (Z + H e^{j\gamma d})Z}{(Z + H e^{-j\gamma d})Z - H^2} e^{-2j(m-1)\gamma d} \end{aligned} \quad (18)$$

Using the relation between the reflection coefficient and current, we get the current matrix as follows:

$$\mathbf{I}_{T2D} = \begin{bmatrix} \mathbf{I}_{11} & \mathbf{I}_{12} & \mathbf{I}_{13} & \cdots & \mathbf{I}_{1k} \\ \mathbf{I}_{21} & \mathbf{I}_{22} & \mathbf{I}_{23} & \cdots & \mathbf{I}_{2k} \\ \vdots & \vdots & \vdots & \cdots & \vdots \\ \mathbf{I}_{i1} & \mathbf{I}_{i2} & \mathbf{I}_{i3} & \cdots & \mathbf{I}_{ik} \end{bmatrix} \quad (19)$$

The current within each tile in the 2-D surface can be calculated by extending the 1-D case separately for the rows and columns. At the intersection tile, we consider the current induced due to the reflected waves in horizontal and vertical directions. We consider next the currents in the different tiles using an example of four tiles with a termination tile (i, k) :

$$\mathbf{I}_{i-1,k} = I(1 + \rho_T^v) \quad (20)$$

$$\mathbf{I}_{i,k-1} = I(1 + \rho_T^h) \quad (21)$$

$$\mathbf{I}_{i-1,k-1} = I(2e^{j\gamma d} + \rho_T^{v,h} e^{-j\gamma d}) \quad (22)$$

$$\mathbf{I}_{i,k} = -\frac{Z}{H} I(1 + \rho_T^{v,h}) - I(2e^{j\gamma d} + \rho_T^{v,h} e^{-j\gamma d}) \quad (23)$$

Based on (20) to (23) and (11), by making the corresponding change $n \rightarrow i$ or k for horizontal and vertical chains, we can obtain current of each tile in the matrix \mathbf{I}_{T2D} .

The received power at the tiles corresponding to the detected objects is calculated as:

$$\mathbf{I}_R \mathbf{R}_L + j\omega \mathbf{M}_{RT} \mathbf{I}_{RT} = 0 \quad (24)$$

$$P_{R-2D} = \frac{\omega^2 \mathbf{M}_{RT}^2 |\mathbf{I}_{TR}|^2}{R_L} \quad (25)$$

where \mathbf{R}_L is a matrix of the resistance of coils in the detected objects. Define \mathbf{R}_T as the resistance of each tile used in the following sections, \mathbf{M}_{RT} is the mutual inductance between receiver coils (abbreviated as ‘receivers’) and the energy tiles of the surface. \mathbf{I}_R , \mathbf{I}_{TR} are the current matrix of detected receivers and energy tiles under the detected receivers, respectively, where $\mathbf{I}_{TR} \subset \mathbf{I}_{T2D}$.

C. Hopping Power Loss

For the $i \times k$ resonating tiles shown in Fig. 4, the total power at each tile P_{tile} can be written as summation of power delivered at the tile and the power loss due to parasitic resistive component within the coil of that tile [32]:

$$P_{tile} = P_{LC} + P_{loss} = \frac{1}{2}(LI^2 + \frac{I^2}{\omega^2 C}) + (\frac{I}{\sqrt{2}})^2 R_{para} \frac{1}{f} \quad (26)$$

where L , C , I , R_{para} are inductance, capacitance, current amplitude, and parasitic resistance of each tile, respectively. Thus, we define the power loss ratio for an energy tile β as follows:

$$\beta = \frac{P_{loss}}{P_{LC} + P_{loss}} \quad (27)$$

Accordingly, the total power over the 2-D surface energy tiles and the receivers is:

$$\begin{aligned} P_{tot2D} &= P_{T-2D}(1 - \beta) + P_{R-2D} \\ &= |\mathbf{I}_{T2D}|^2 \mathbf{R}_T(1 - \beta) + \frac{\omega^2 \mathbf{M}_{RT}^2 |\mathbf{I}_{TR}|^2}{\mathbf{R}_L} \end{aligned} \quad (28)$$

where P_{T-2D} is the total power of all energy tiles. The surface charging efficiency is computed as:

$$\eta_{2D} = \frac{P_{R-2D}}{P_{T-2D} + P_{R-2D}} \quad (29)$$

We explain next our approach to optimize the wireless power transfer to multiple devices on/over the 2-D surface. The main challenge is to maximize the received power at the detected devices while minimizing the total transmitted power of the system and hopping power loss. We use 2-D models developed in this section such as total received power, total transmit power, and current based on the power reflections to find solutions for optimal surface energy transfer, and adaptive energy hopping.

V. OPTIMIZING SURFACE ENERGY HOPPING

From (28), the total power is equal to $P_{tot2D} = P_{T-2D}(1 - \beta) + P_{R-2D}$. Since β depends on the coil hardware characteristics and the main objective is to maximize power delivery to the receiver coils, P_{tot2D} is minimized when P_{T-2D} is minimized.

Given total transmit power of the amplifier in the master tile is adjusted based on total load of receivers [33] and the number of active tiles, this problem reduces to minimizing the number of active energy tiles. SoftCharge achieves this by choosing the active paths from source to detected receivers as well as by blocking the energy over tiles that are not part of the

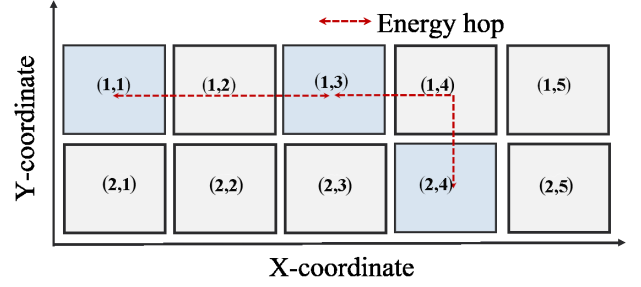


Fig. 5. Sample scenario of energy hopping, with energy blocking and energy cancellation.

active paths (Theorem II). Accordingly, the main challenge can be deconstructed into three problems (i) how to find optimal energy paths, called as *active paths*, from source to multiple destinations, (ii) how to remove the reflections within each path to maximize the received power, and (iii) how to block power for energy tiles on other paths that are not part of active paths.

Next, we introduce two theorems to provide exact solutions to maximize the received power and minimize the total transmit power. The proofs are provided in Appendix.

Theorem 1: Given active energy paths $\mathbf{P} = \{\mathbf{P}_1, \mathbf{P}_2, \dots\}$ and energy tiles $\mathbf{T}_a = \{\mathbf{T}_1, \mathbf{T}_2, \dots\}$ in each active path \mathbf{P}_a , the received power is maximized for the receivers when the impedance of termination tiles in \mathbf{P}_a is set to: $C_a = C + \Delta C_a$, where $\Delta C_a = \frac{1}{\omega^2 M}$.

Theorem 2: Given active energy paths $\mathbf{P} = \{\mathbf{P}_1, \mathbf{P}_2, \dots\}$ and set Λ^T consists of all energy tiles p in each path \mathbf{P}_a , $\mathbf{T}_q = \{\mathbf{T}_1, \mathbf{T}_2, \dots\}$ are tiles that are in surface and not member of Λ^T . The total transmitted power can be minimized if the transmitted power is blocked on each tile q in \mathbf{T}_q , and the capacitance is set to $C_q = C + \Delta C_q$ for each tile in order to block the transmitted power at this tile, where: $\Delta C_q \geq \left| \frac{|\mathbf{I}_q|^2 - \epsilon Z_q}{j\omega} \right|$.

A. Sample Scenario of Energy Blocking and Cancellation

This section gives an overview of a sample use case involving energy hopping using Fig. 5. We discuss the roles of energy cancellation caused by MI wave reflection and energy blocking that directs the energy transfer along specific tiles. Due to the MI wave reflection, the magnetic field at specific tiles is equal in amplitude but with opposite direction, which leads to the energy cancellation. As shown in the Fig. 5, we place ten tiles in two rows, with the tuple (i, k) representing the tile at i^{th} row and k^{th} column, respectively. Tile $(1, 1)$ is the tile connected to the AC power source. The tiles in the set $\{(1, 1), (1, 2), (1, 3), (1, 4), (2, 4)\}$ form the energy hopping path, although only $\{(1, 1), (1, 3), (2, 4)\}$ can support charging devices placed on them. Tiles $(1, 2)$ and $(1, 4)$ are energy cancellation tiles but the coupling with other tiles remains the same. The energy canceled tiles with other unaffected tiles form the energy path. Of the remaining tiles, the set $\{(1, 5), (2, 1), (2, 2), (2, 3), (2, 5)\}$ lose the mutual coupling with other tiles and they do not belong to the energy path. As a result, they are blocked from the energy flow path. The

mathematical theory of (i) energy blocking and (ii) energy cancellation are explained following:

1) *Energy Blocking*: The operation of energy blocking is explained in (49)-(52), when the power delivered is below ϵ . In such a condition, the impedance change of each tile is given in (52).

2) *Energy Cancellation*: Consider the last three tiles in the energy hopping path that terminates with (2,4), We first express the current distribution in these tiles using (10)-(12):

$$\mathbf{I}_{24} = -\frac{Z}{H}I(1 + \rho_T) - I(e^{j\gamma d} + \rho_T e^{-j\gamma d}) \quad (30)$$

$$\mathbf{I}_{14} = I(1 + \rho_T) \quad (31)$$

$$\mathbf{I}_{13} = I(e^{j\gamma d} + \rho_T e^{-j\gamma d}) \quad (32)$$

As explained in previous works [30], [31], Z is assumed to be zero during wireless charging. When there is no impedance change, $\rho_T = -1$ according to (12), so the current of \mathbf{I}_{14} is zero, and the current magnitude of \mathbf{I}_{13} and \mathbf{I}_{24} are same. Then, the tile (1,3) is the new imaginary termination of first three tiles because of the cancellation of tile(1,4) Using the same methodology for last three tiles, the current distribution is expressed as:

$$\mathbf{I}_{13} = I(e^{j\gamma d} + \rho_T e^{-j\gamma d}) \quad (33)$$

$$\mathbf{I}_{12} = I(1 + \rho_T) \quad (34)$$

$$\mathbf{I}_{11} = -\frac{Z}{H}I(1 + \rho_T) - I(e^{j\gamma d} + \rho_T e^{-j\gamma d}) \quad (35)$$

when Z doesn't have any change, current \mathbf{I}_{12} is zero, and the current magnitude \mathbf{I}_{11} and \mathbf{I}_{13} are same. Summarizing, we obtain the current distribution of these five tiles, and we find that the first, third, and five tile have same magnitude of current. The second and fourth tiles are impacted by reflection from the termination tiles thereby nullifying their action. The set of tiles $\{(1, 5), (2, 1), (2, 2), (2, 3), (2, 5)\}$ is blocked with the impedance change.

B. Adaptive Energy Hopping

Theorem 1 and Theorem 2 provide the analysis of how to maximize the received power of each tile in each path \mathbf{P}_a and how to block the energy tiles that do not belong to \mathbf{A}^T . Section 5.1 clarifies the difference between energy cancellation and energy blocking of each each tile. Given a detected object, we explain an algorithm for adaptive energy hopping, the determination of the active path, minimizing the number of hops, and blocking the tiles outside the power flow path. As explained earlier, the energy tiles have i rows and k columns, with termination tile (i, k) .

Consider the energy tiles (ETs) written in a matrix \mathbf{ET} , with the subscripts indicating the location of a particular tile:

$$\mathbf{ET} = \begin{bmatrix} ET_{11} & ET_{12} & \cdots & ET_{1k} \\ ET_{21} & ET_{22} & \cdots & ET_{2k} \\ ET_{31} & ET_{32} & \cdots & ET_{3k} \\ \vdots & \vdots & \vdots & \vdots \\ ET_{i1} & ET_{i2} & \cdots & ET_{ik} \end{bmatrix} \quad (36)$$

Assuming the location of device via sensing feedback is ET_{uv} , $(u, v) \subset (i, k)$. From tile (1, 1) to tile (u, v), the active

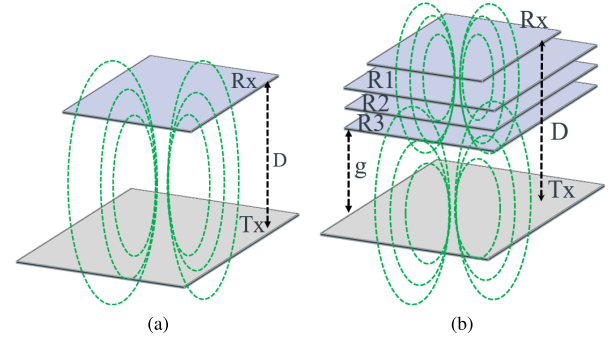


Fig. 6. The reconfigurable receiver is composed of final load receiver Rx (a) and multiple relay coils R1-R3 as shown in (b). Tx is the coil of the energy tile directly under the given surface.

path is confirmed by the simple way that energy flow path starts from tile(1, 1) to (1, v) along first row and then go from tile (1, v) to tile (u, v) along v_{th} column. Then active path is expressed as:

$$\mathbf{P}_a = [ET_{11} \quad ET_{12} \quad \cdots \quad ET_{1v} \quad ET_{2v} \quad \cdots \quad ET_{uv}] \quad (37)$$

and total number of energy tiles that the MI wave must pass through is $P_{num} = u + v - 1$. According to our derivations on current cancellation due to reflected waves and energy blocking, we obtain the optimized number of active energy tiles and the corresponding protocol, named as EH_{opt} as follows.

$$EH_{opt} = \begin{bmatrix} 0 & \text{if } u + v = 2 \\ 1 & \text{if } u + v = 3 \\ 1 & \text{if } u + v = 4 \\ 2 & \text{if } u + v = 5 \\ u + v - 4 & \text{if } u + v \geq 5 \end{bmatrix} \quad (38)$$

Then energy tiles of $\mathbf{T}_a = \mathbf{P}_a$, and the tiles that need to be blocked are $\mathbf{T}_q = \mathbf{ET} - \mathbf{T}_a$

VI. RE-CONFIGURABLE MULTI-COIL RECEIVER

The previous sections explain how to deliver power to a specific energy tile through energy hopping. However, large objects, such as UAVs can only be charged at limited vertical distance from that tile, typically around 20 cm. For the use-cases where the receiver's charging framework can also be controlled, i.e., when the receiver also runs SoftCharge, then we can further optimize the power delivery through reconfiguration of the coils at the receiver end. The main idea, as shown in the Fig. 6(a-b), is to have multiple receiver coils, and specific number of coils that should be excited depends upon the height of the object from the transmitter energy tile.

The enhanced receiver design is composed of a single load receiver coil (Rx) and several multi-relay coils that are placed below it (R1-R3), where we use three coils in our example, as shown in Fig. 6. The separation between any one of relay coils and receiver coil at the receiver side is dx , such as the distance between R1 and Rx, R1 and Rx or R3 and Rx. The direct transmitter coil (Tx) to Rx distance is D , and the Tx to the first resonating layer distance is g . Hence, $D = g + dx$.

The multi-coil receiver is useful for situations where the power delivery needs to remain within bounds at all times,

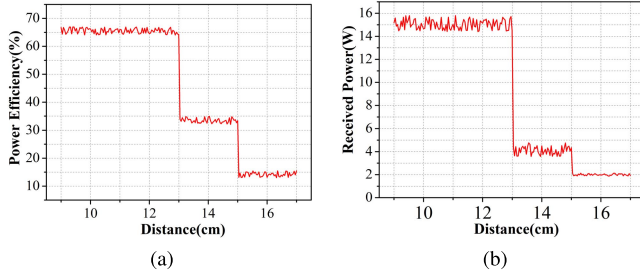


Fig. 7. (a) Varying distance g changes the efficiency of power transfer at the load receiver coil, and (b) UAV wireless charging with different resonant relay coils R1, R2, R3 as shown in Fig. 6.

for example, depending on the type of the object/UAV, its battery capacity etc, and its aerial height, a specific relay coil (R1-R3) is activated. We show in our experimental studies that the power transfer range extends $5\times$ through this approach compared to the single Tx-Rx transfer. We analyze the multi-coil receiver using similar analytical approach used to explain energy hopping.

The electro-magnetic relationship between the Tx and Rx, with an intermediate relay coil R_R can be expressed as:

$$\mathbf{V}_{Tx} = \mathbf{I}_{Tx}(j\omega L_{Tx} + \frac{1}{j\omega C_{Tx}} + Z_{Tx}) - j\omega M_{TxRx} \mathbf{I}_{R_R} \quad (39)$$

$$\mathbf{I}_{R_R}(j\omega L_{R_R} + \frac{1}{j\omega C_{R_R}} + Z_{R_R}) + j\omega M_{TxR_R} \mathbf{I}_{Tx} + j\omega M_{R_R R_R} \mathbf{I}_{R_x} = 0 \quad (40)$$

$$\mathbf{I}_{R_x}(j\omega L_{R_x} + \frac{1}{j\omega C_{R_x}} + Z_{R_x} + R_{Load}) + j\omega M_{R_x R_R} \mathbf{I}_{R_R} = 0 \quad (41)$$

where, V_{Tx} , L_{Tx} , C_{Tx} , and Z_{Tx} represent the voltage, inductance, capacitance, the impedance from energy tile Tx, respectively. M_{TxR_R} gives the mutual inductance between Tx and a given receiver relay coil (from R1 to R3, in our case). L_{R_R} , C_{R_R} , and Z_{R_R} are inductance, capacitance, impedance of that chosen relay coil, respectively. Similarly, L_{R_x} , C_{R_x} , Z_{R_x} and R_{Load} are inductance, capacitance, impedance and load resistance of final receiver coil. At resonance state, the effect of L and C cancel each other. Combining (39) with (41), we express the power efficiency as:

$$\eta = \frac{|j\omega M_{TxR_x}|^2}{R_{Load} Z_{Tx}} \quad (42)$$

From (42), we see that the power efficiency is only related to the mutual inductance between coils, which is a function of distance between coils. So, for a given receiver-relay coil arrangement, the power efficiency is expressed as $\psi_R = f(g, dx)$. In our design, the size of transmitter and relay coils at the receiver is the same, but the load receiver coil is smaller. This makes the change in M_{TxR_x} much bigger than the change of $M_{R_x R_R}$. This implies that any change in g influences power efficiency to a greater extent than a change in dx . Fig. 7a shows the experimental results how efficiency changes with the different distance g between a single relay coil R3 (coils R1 and R2 are switched off) and the energy tile in an experimental setup. The load receiver coil Rx is kept constant at 20cm in all cases, with the intermediate relay

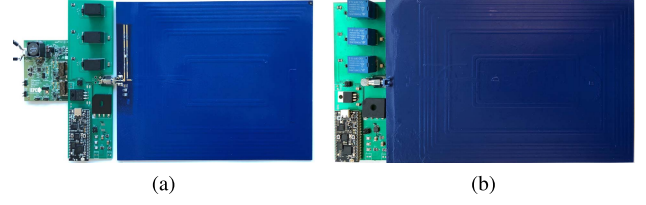


Fig. 8. SoftCharge implementation with (a) master energy tile, with PCB integrated with the charging coil and the power amplifier, and (b) top view of the slave energy tile.

moved from 9-17cm. We see a step-wise efficiency drop, this is because the mutual inductance between transmitter and relay coils exponentially drops when the distance between them increases [34]. Additionally, the power efficiency between transmitter and relay significantly drops as it depends on the mutual inductance. Our goal of the multi-coil relay is to boost the efficiency at these *knee* points. Fig. 7b shows the actual received power levels for three different resonant relay coils R1, R2, R3 as shown in Fig. 6.

VII. SYSTEM IMPLEMENTATION

We implement SoftCharge with off-the-shelf coils and power amplifiers, with additional PCB fabrication and interfacing of circuit components to create master and slave energy tiles as shown in Fig. 8. In the system we use Class-D amplifier [33], [35] as an AC source to provide power to energize the master tile, though significant additional efficiency improvement can occur with custom-designed amplifiers, which we leave for future work. The output power is limited to 30W in this paper, although, we have tested the setup up to 110W without any impact on the performance.

Each tile also runs the SoftCharge software stack that performs sensing and energy hopping related optimizations. Each tile mainly consists of three parts, the customized PCB control part, energy transfer coil and sensing coil. Each PCB control circuit consumes less than 200-250 mW, with an average of 100 mW to collect sensing data and 100-150 mW for switching. The control circuit power consumption is 100-150 times less than the amplitude of the wireless transfer power. Accordingly, the overhead of control circuitry power consumption on the wireless power transfer efficiency is negligible. The large blue areas in Fig. 8 cover the actual energy transfer coil that resonates at 6.78MHz with inductance $4.8 \mu H$ and compliant with the frequencies specified by the AirFuel Alliance [3]. In addition, each individual energy tile has an additional 150KHz resonance coil for sensing. This is the same frequency used in the Qi standard. We build sensing coils with the specifications of AWG 17 (1.15 mm diameter) type 2 litz wire having 105 strands of 0.08 mm diameter, which is same as the wire used in Qi-standard transmitter coil. The impedance controller receives directives from the software control plane, and adjusts capacitance of the tile accordingly.

We leverage Thread protocol [36] to create a full-mesh network among the tiles. Thread is a mesh networking protocol for low-power IoT devices. It uses 6LoWPAN and IEEE 802.15.4 for communication with 2.4GHz frequency band. We use the mesh development kit nRF52840-MDK(32-bit

TABLE I
PARAMETERS IN PCB FABRICATION AND FABRICATION COMPONENTS
FOR MULTI-COILS SENSING PROTOTYPE

Component	Value	
PCB	Size	15.1cm x 5.1cm
	Trace width	1 mm
	Dielectric constant	4.6
	Through-hole size	1 mm
μ CU	nRF52840-MDK	32 bit ARM Cortex-M4 72 MHz CPU
Switch	Solid-state Relay	Omron G3VM-101CR IOR PVAZ172N
Sensing Wave Generator	555Timer	Texas Instruments
Regulator	LT1076-5	Linear Technology
Resonator Capacitor for Sensing Coils	Ceramic Capacitor	56 pF
Resonator Capacitor for MR Charging Coils	Ceramic Capacitor	5,7.5,330 pF

ARM CortexTM-M4 CPU) as microcontroller that uses an open-source implementation of Thread protocol provided by Google – OpenThread [15]. Each MDK node acts as a Thread Router resulting in creating a full-mesh network of the tiles. Being resilient to failures, self-organizing, and energy-efficient makes Thread an apt choice for connecting the SoftCharge tiles.

The waveform generator outputs a square-wave signal of amplitude 5 V at 150kHz to excite the circular inner coil. The coil starts to resonate with the outer passive coil. The voltage rectifier converts the induced magnetic field signal at the outer coil into functional DC voltage. The presence of a device near the outer coil affects the mean and variance of the magnetic field. The resulting voltage drop at the output of voltage rectifier is converted by the ADC in the microcontroller into digital format, which is used to detect the type of device. The overall process can be summarized as follows. At the start, the PCB digital controller unit in each tile is switched on. The tiles configure themselves into a mesh network via OpenThread and each slave initiates contact with the master tile. At this stage, each tile is ready to sense voltage variations on the sensing coils and report measurements to the master tile. On receiving these values, the master performs a number of computations: It calculates which tiles have a device to be charged, the optimum energy path, the choice of capacitance for each tile based on the blocking and cancelling Theorems in Section V. The latter parameter is then broadcast to all the tiles that form the mesh network. Each tile now selects the appropriate capacitor to begin the energy hopping process. We design a 4-layer receiver for UAV charging. Overall each energy tile along with the attached PCB unit measure 16cm × 28cm dimensions. Additional details of the energy tile implementation are listed in Table. I.

VIII. EXPERIMENTAL RESULTS

We attach upto 8 energy tiles under a wooden desk with dimension of 72cm × 52cm and thickness 4cm, although for different tests the exact number of tiles can vary. We use iPhone 8, iPad, 13 inch MacBook Pro, and Solo 3DR UAV as the test devices for sensing and charging. The receiver coil and circuit attached to these objects, and we do not make any modifications to them in either the hardware or software.

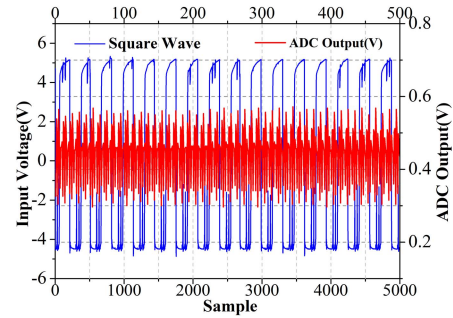


Fig. 9. A 150 kHz square wave excitation signal applied to the inner coil (blue line) and (red curve) the resulting induced voltage at the output of the ADC in the outer coil with sampling rate set at 10^4 samples/s.

TABLE II
VOLTAGE CHANGES FOR DIFFERENCE DEVICES AT THE OUTER COIL

Device	Phone	UAV	Tablet	Laptop
Voltage Change(mV)	120	70	150	290

A. SoftCharge Contact-Less Sensing

This section evaluates the performance of our resonance-based contact-less sensing. To understand the impact of a nearby object in the induced voltage at the outer coil, we consider first the initial conditions where the magnetic field is completely undisturbed. With the sampling rate set at 10^4 samples/s, the blue curve in Fig. 9 shows the excitation signal applied to the inner coil during 50ms, which induces a time varying AC voltage at the outer coil with 5 V peak to peak amplitude. This voltage at the outer coil is converted by the ADC to digital values and analyzed by the microcontroller in real time. With same sampling rate as blue curve, Fig. 9 red curve shows the DC voltage output from the ADC during 500 samples. This is the baseline signal on which SoftCharge attempts to identify variations. It has a clear peak-to-peak range, from 0.55 V to 0.3 V. We average the measurements per 10 samples to avoid false alarms due to transient fluctuations. We test with the four devices successively at 4cm height from the energy tile, as described earlier, with the resulting voltage variations in each case shown captured through the sample count in Table. II. The laptop shows the highest voltage change. Interestingly, the UAV has similar dimensions as the laptop, but it has less coverage with the sensing coil. This gives the smallest voltage change. Similarly, the phone and iPad show corresponding voltage changes proportional to their dimensions. The current version of SoftCharge does not aim to identify the type of objects but simply detect them above an energy tile, we infer that the sensing approach is sensitive to the presence/absence of a target object. In our previous work [37], we focused on using contact-less sensing specifically for object type detection.

B. Energy Hopping and Optimization

We first test SoftCharge gives expected results along a 1-D array, before starting an extensive campaign of 2-D tests. For initial testing, we place five identical tiles arranged as a straight line with 1.5 cm gap between each pair of coils.

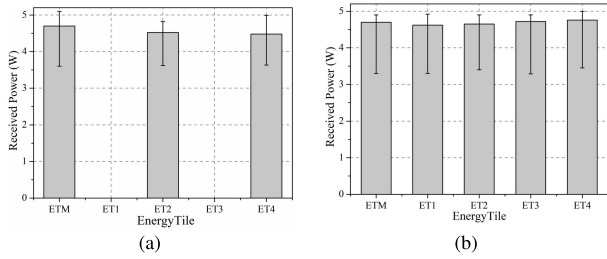


Fig. 10. 1-D Energy hopping (a) received power distribution from each ET without impedance optimization, (b) received power distribution from each ET with impedance optimization.

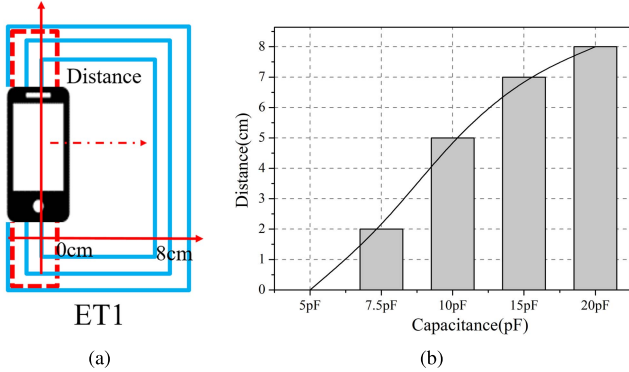


Fig. 11. Impedance optimization based Controllable Area Charging. (a) represents the charging area and (b) shows charging area change with different capacitance.

We start by connecting each coil in series with a resonant matched capacitor to set the resonant frequency at 6.78MHz, without any hardware or software changes in the amplifier, transmitter/receiver coils. A phone with a receiver coil attached to it is moved over each tile, at a fixed height of 4 cm. We observe that the maximum received power is 5 W, although not all the energy tiles (abbreviated henceforth as ET) are able to charge the phone, as shown in Fig 10a. ET1, ET3 and ET5 deliver approximately same power, but the power from ETs 2 and 4 is zero because of the wave reflection, as explained from Sec. IV-B. To ensure that the user can freely charge from any tile, we need to use the impedance optimization framework in Sec. V to eliminate the reflected wave.

1) *Eliminating the Energy Cancellation*: Energy cancellation is caused by MI wave reflection, and the reflection is a function of impedance change as explained in (44)-(46). We tested first 3 ETs (ETM, ET1 and ET2) in experiments to find the optimized impedance change and then we apply this to 5 ETs configuration. In the chain of 3 tiles with configuration that ET2 is chosen as the termination tile and there is no any impedance change on ET2, ETM and ET2 deliver approximately 5W, and ET1 is cancelled. When changing the capacitance of ET2, we see that the received power from ETM and ET2 is around 5 W at any location in the tile, although the power from ET1 varies. In Fig. 11a, the red dashed square represents the charging area that is proportional to the distance from left edge (0 cm) to right edge (8 cm). In the experiments, a phone moves from the left edge to right edge. Fig. 11b shows the width of ET1 charging area as a

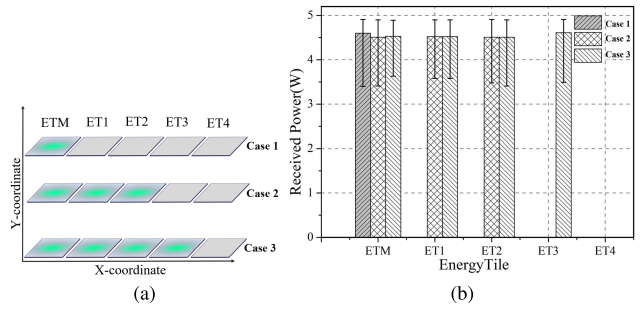


Fig. 12. (a) Three cases of energy blocking with different combination from ETM to ET4 and (b) the corresponding received power of each ET.

function of capacitance change of ET2. The results show that the receiver over ET1 can get same power at any location of this tile as well as the same received power distribution over all three ETs, when the capacitor change of ET2 is 20pF. Similarly, this can be applied into chain of 5 ETs by changing the capacitor of termination tile. The received power from each ET is shown in Fig. 10b. Compare results in Fig. 10a and Fig. 10b, each ET has same ability to transfer power with capacitance optimization. The capacitor change of 20pF is in parallel to the existed capacitors by converting to the capacitance change, our experiment reveals that the required change in capacitance to induce a corresponding impedance change is $\Delta Z = 7.93 \Omega$. The analytical values calculated in (48) is $\Delta Z = 8.13 \Omega$. The error between them is only 0.2Ω , which shows there is strong agreement between our analysis and experiments.

2) *Energy Blocking*: Our analysis presented in (51) and (52), shows that the energy tile power relaying and delivery falls drastically, when the chosen capacitance value is far from the value that achieves resonance. We call this as *energy blocking*. In the 1-D arrangement of tiles, we demonstrate the blocking concept when we set the capacitance as 330 pF for those tiles that should not participate in the energy hopping process. In order to eliminate the energy cancellation, we also set the 330pF capacitor in parallel with the existing capacitor. As shown in Fig. 12a, we test three cases:

- The master tile ETM can only deliver power. Thus, the pathway ET1-ET4 should be blocked. We select the 330 pF capacitor at ET1-ET4 to achieve this goal.
- ETM, ET1 and ET2 should deliver power. For this case, the termination tile selects 20pF to smooth the power distribution among these three tiles, while ET3 and ET4 is connected to a 330pF capacitor to block power flow further down the chain.
- Only ET4 should not deliver power but the rest should. For this case, ET2 and ET4 are connected with a 20 pF and 330 pF capacitor to reduce the MI wave reflection and block power transfer separately. After the capacitance optimization, Fig. 12b shows the received power of each ET at the phone for three cases. We see that the blocked ET is unable to transfer any power.

By combining the concepts of energy blocking with impedance optimization, we now turn our attention towards full energy hopping in a 2-D plane.

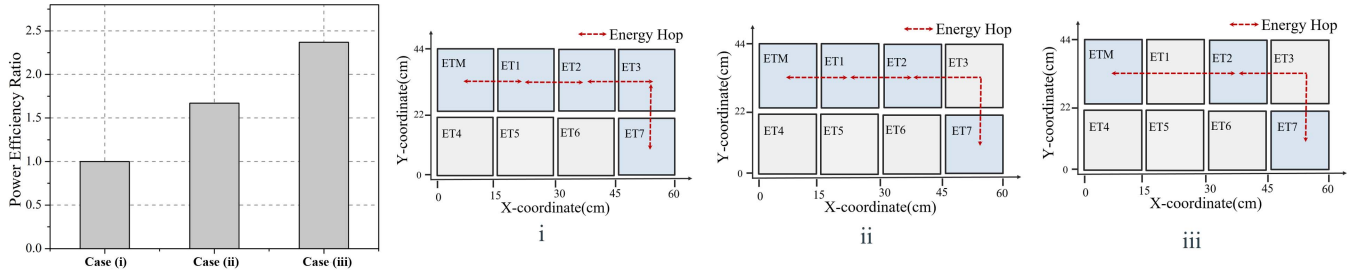


Fig. 13. Power efficiency ratio with different hops and the corresponding illustration.

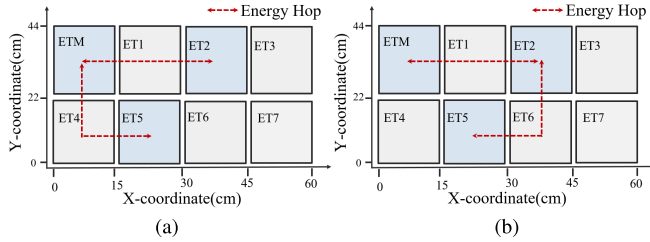


Fig. 14. Multi-device charging scenarios for two devices that are located at ET2 and ET5 with two different case: (a) two paths and (b) one path.

3) *Energy Hopping and Tile Optimization*: Consider 8 energy tiles arranged in 2×4 array. As sensing stage precedes the wireless transfer, we know which tiles participate in concurrent energy delivery. The discussion below follows from the algorithm described in Sec. V.

Fig. 13 shows the results of power efficiency for three different active tiles scenarios that 8 energy tiles are arranged in two rows of four tiles each. The optimal energy flows from the master energy tile (ETM) to a device located at ET7 crosses multiple tiles. For each scenario, the energy tiles can be re-configured such that the power on selected tiles over an active energy flow path be cancelled through guiding MI wave reflections with impedance optimization or blocked through power blocking, as discussed in Section V-A. Here, the receiver is located at ET7 and the active path from ETM to ET7 crosses multiple tiles names in the set $\{ETM, ET1, ET2, ET3, ET7\}$ with termination tiles (ET7) and imaginary termination tile (ET2) according to the explanation of Section IV(B). The tile set of $\{ET4, ET5, ET6\}$ is blocked by connecting the 330pF capacitor for each of the tiles. The shaded blue tiles indicate those tiles that are neither cancelled nor blocked from power delivery. For simplicity, the power efficiency ratio is normalized. We observe that optimal re-configuration of energy tiles can improve the power efficiency on this example experiment upto 2.4 times.

4) *Multi-Device Energy Hopping Optimization*: Previous experiments involved one device charging at a time. Fig. 14a and Fig. 14b show two energy hopping cases when two devices are being charged at the same time over a grid of 8 energy tiles that are arranged horizontally in two rows of four tiles each. Here, the devices that are located over ET5 and ET2 need power at the same time. In case one (Fig. 14a), two different paths are used and ETM needs two mutual couplings to transfer power along these two different paths. Energy tile ET3, ET6 and ET7 are blocked by setting impedance to

TABLE III
RESULTS OF TWO DIFFERENT CASES CORRESPONDING TO THE DIFFERENT PATHS FROM FIG. 14

Device	Case 1	Case 2
Power Efficiency Ratio	1	1.55

330 pF, and power at ET1 and ET3 is cancelled. While in case two (Fig. 14b), one path is used, and ETM only needs one mutual coupling to pass the power to next tile, which increases the end-to-end power efficiency. ET3, ET4, ET7 are blocked by connecting them to a 330 pF capacitor, ET1 and ET6 is cancelled. Table. III shows the results for two cases and indicates that case two is 1.6 times more energy efficient than case one. This result demonstrates the importance of optimal energy hopping over multiple receivers.

IX. COMPARATIVE END-TO-END APPLICATION TRIALS

In this section, we demonstrate complete end-to-end application performance that includes a mesh network that connects the ETs, and combine the functions of sensing and hopping as one integrated framework. We compare SoftCharge with the state of the art, such as HotSpot charging, Qi charging and MagMIMO charging, which are reviewed in Sec. II. Finally, we report on the charging performance for multiple objects, phone, tablet, laptop and UAV (with reconfigurable receiver) using the SoftCharge approach. We use the same 2-D set up as described earlier with 8 coils, with the tile identifiers corresponding to their locations in the coordinate plane. Alongside the wooden table, we study the effect of other materials like plastic and glass. For the phone charging experiment, for lack of space, we show results from only one phone placed on tiles 3, 4, 5, and 6 in turn. We allow SoftCharge to complete the sensing and energy hopping as defined in the previous sections, which minimizes hops. Fig. 15a shows the received power at the phone at 4cm height for each of these separate trails, when the surface is switched to different materials.

We next compare the charging time of the phone from a fully depleted to charged state as shown in Table. IV. Each of these alternate methods are adapted for 5W configuration. We see that SoftCharge exhibits faster charging performance. Compared to Qi, SoftCharge not only improves charging distance by $6\times$ but also covers over $100\times$ larger charging area using only 8 ETs. Though MagMIMO also shows a good charging performance, it uses 6 amplifiers and 6 transmitter coils covering $0.38m^2$ charging area. As opposed to this,

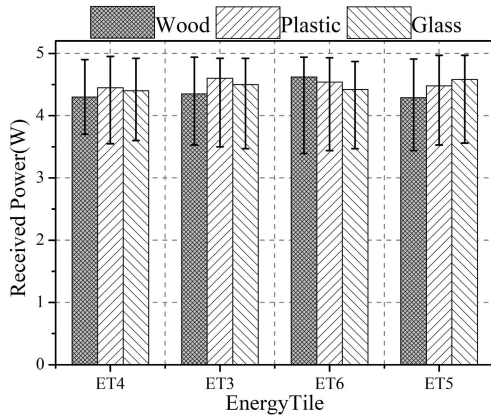


Fig. 15. 2-D surface charging evaluation with four different positions of phone and the received power.

TABLE IV
CHARGING TIME COMPARISON AMONG HOTSPOT, Qi, SOFTCHARGE AND MAGMIMO

Method	Hotspot	Qi	SoftCharge	MagMIMO
Charging time (mins)	118	170	105	150

SoftCharge only uses one amplifier powering 8 ETs to cover the same area of charging ($0.374m^2$), with a higher charging rate. HotSpot charging speed is lower than SoftCharge, and it can only charge comparatively low power devices, like a phone and watch. SoftCharge is flexible in the low-to-high power delivery range, and can also charge laptops, UAV with reconfigurable receiver.

We next extend testing of SoftCharge for different objects, such as tablet, laptop, and UAV. For the tablet, we use 5V receiver, and the for laptop and UAV, we use 19V receiver. Similar to phone sensing and charging, the tablet, laptop and UAV can be freely placed anywhere in the 2-D plane, and we maintain the earlier height of 4cm (save for UAV, we test at 20cm as it has a reconfigurable receiver). Figs. 16 demonstrates the received power for four different devices, where each device is placed at ET4. We experimentally observe a maximum power of 5 W for phone, 6 W for tablet, 23 W for laptop, and 16 W for UAV over different materials. Some results are as expected: for example, a larger coil increases the received power, allowing the laptop to receive maximum 23 W while phone and tablet with the smaller coil only getting 5 W. The larger coil has more magnetic flux coupling that induces greater current in the coil. For the UAV, even at the charging distance if 20 cm, with the optimization through multi-layer receiver coil configuration, we can get 16 W. The surface composition material does not significantly affect the charging performance.

Next, we study in more depth the UAV charging with the relay coil receiver. We evaluated the received power with different positions of layers and different rotational angles with respect to the horizontal surface, as shown in Fig. 17a to Fig. 17c. Fig. 17d shows the results of how the received power changes with distance and different rotational angle α visually seen in Fig. 17a. Interestingly, we see that

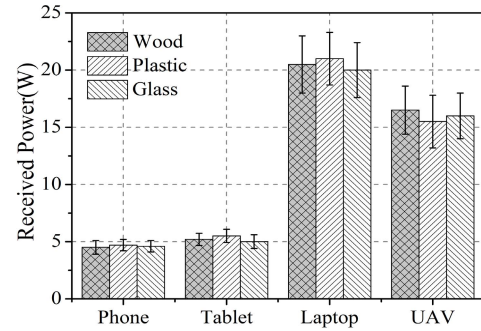


Fig. 16. Maximum received power for phone, tablet, laptop, and UAV devices located at ET4 over different materials.

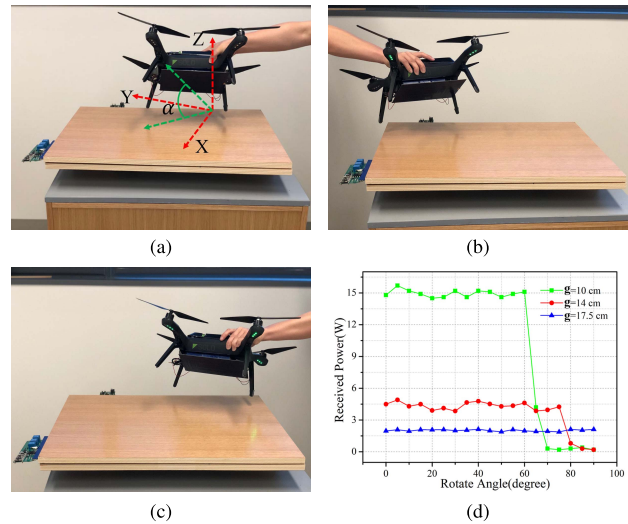


Fig. 17. UAV wireless charging with different rotate angle and distance, (a) visually shows the UAV rotational angle and (b), (c) at different position with same rotational angle and distance, (d) received power with different rotational angle and distance.

short g gives higher power but has less rotational flexibility as opposed to higher values of g . For example, when g is 17.5 cm, the permissible rotational angle is 25 degrees more than the case when g is 10 cm. Based on our evaluation, we can see that SoftCharge can transfer power to different devices with different charging distances, is able to charge multiple devices at the same time, and is also robust to angular variations between coils.

X. CONCLUSION

This paper introduces SoftCharge, first of its kind software-defined wireless charging system that transforms an existing surface into an on-demand multi-device power transmitter. It consists of magnetic resonance sensing system and energy hopping wireless power transfer system over large surface. We develop the theory of energy hopping over 2-D surface by adjusting coil-impedance through using software directives. SoftCharge supports mW contact-less sensing over a large surface within milliseconds and charges multiple types of devices such as phone, tablet, laptop, and UAVs. The re-configurable multi-layer receiver configuration can potentially extend the charging distance to 20 cm, with up-to 16 W

received power. Additionally, our approach can support up-to 85° angular difference between the coils without interrupting charging. In our future work, we will incorporate theoretical enhancements that will allow us to detect the specific type of objects. This will allow us to deliver optimized power. We will also study the effect of changing object locations over time and further improve efficiency by exploring optimizing coil dimensions for generic device sensing and charging.

APPENDIX

A. Proof of Theorem I

Similar to (25), the maximized received power for all receivers located on \mathbf{P} can be formulated as:

$$P(\text{Max})_{R-2D} = \frac{\omega^2 \mathbf{M}_{RT}^2 |\mathbf{I}_{TP}|^2}{\mathbf{R}_L} \quad (43)$$

where \mathbf{I}_{TP} is the matrix of energy tiles in \mathbf{P} that are directly located under the receivers. Given that the distance between tiles and physical characteristics of coils (M_{RT} and ω) stays the same, the maximization of received power translates into maximizing the currents of the energy tiles. As explained in (16) and (17), current distribution either in horizontal or vertical chain of tile is a function of ρ_T . Since the reflection coefficient ρ_T is always a negative number, the total current maximization happens when ρ_T for all tiles in the active path becomes zero and thus wave reflections are eliminated. For simplicity, we use ρ_T to represent all the reflection of row or column instead of ρ_T^h or ρ_T^v in 2-D surface, since they are equal, as explained in section IV-B.

The reflection coefficient can be written as a function of impedance change ΔZ as follow:

$$\rho_T(\Delta Z) = \frac{H^2 - (Z + He^{j\gamma d})(Z + \Delta Z)}{(Z + He^{-j\gamma d})(Z + \Delta Z) - H^2} \quad (44)$$

and rearranging the above equation we get:

$$\Delta Z(\rho_T) = \frac{(H^2)(1 + \rho_T)}{Z(1 + \rho_T) + H(\rho_T e^{-j\gamma d} + e^{j\gamma d})} - Z \quad (45)$$

As discussed before $Z = 0$ and the required impedance change to remove the reflections for $\rho_T = 0$ is:

$$\Delta Z(\rho_T) = He^{-j\gamma d} = j\omega M e^{-j\gamma d} \quad (46)$$

Recall that resonant state is defined as the condition where the working frequency is equal to the resonating frequency of each tile. With the case that the mutual coupling happens in the sub-wavelength, we have $e^{-j\gamma d} = -1$ and $\gamma d = \pi$ that results in the amplitude $\Delta Z(\rho_T)$ equalling to ωM with the imaginary phase angle as 90°.

The optimal impedance and capacitance change to maximize the current of an energy tile, which maximizes its received power is:

$$\Delta Z(\rho_T) = -j\omega M = \frac{1}{j\omega \Delta C_a} \quad (47)$$

$$\Delta C_a = \frac{1}{\omega^2 M} \quad (48)$$

B. Proof of Theorem II

Consider tile p and tile q as a pair of neighbour tiles with strong coupling. Using circuit theory, we express their current and voltage relationships as follows:

$$\mathbf{V}_p = \mathbf{I}_p(j\omega L_p + \frac{1}{j\omega C_p} + Z_p) - j\omega M_{pq} \mathbf{I}_q \quad (49)$$

$$\mathbf{I}_q(j\omega L_q + \frac{1}{j\omega C_q} + Z_q) + j\omega M_{pq} \mathbf{I}_p = 0 \quad (50)$$

where \mathbf{V}_p , \mathbf{I}_p , \mathbf{I}_q , L_p , L_q , C_p , C_q , Z_p , Z_q and M_{pq} are the voltage, current, inductance, capacitance, impedance, and the mutual inductance between these two tiles. The power in the tile q with capacitance change ΔC_q would be:

$$P_q = |\mathbf{I}_q|^2 \frac{1}{j\omega L_q + \frac{1}{j\omega C_q} + j\omega \Delta C_q + Z_q} \quad (51)$$

Here, we consider the tile q is blocked when its delivered power becomes ϵ . By substituting ϵ into P_q , we get the minimum capacitance change required as:

$$\Delta C_q = \left| \frac{|\mathbf{I}_q|^2 - \epsilon Z_q}{j\omega} \right| \quad (52)$$

Any capacitance change that is bigger than ΔC_q blocks the energy hopping through this coil.

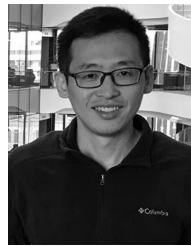
ACKNOWLEDGMENT

This work is supported by the funds available through the US National Science Foundation award CNS 1452628.

REFERENCES

- [1] N. Tesla, "The transmission of electric energy without wires," *Electr. World Eng.*, vol. 5, pp. 162–167, Apr. 1904.
- [2] W. P. Consortium. (2018). *Qi-Mobile Computing*. [Online]. Available: <https://www.wirelesspowerconsortium.com/qi/>
- [3] A. Alliance. (2014). *Airfuel Resonant Specification*. [Online]. Available: <https://www.airfuel.org/>
- [4] D. W. Baarman, "Laptop and portable electronic device wireless power supply systems," U.S. Patent 8164222, Apr. 24, 2012.
- [5] S. Lukic and Z. Pantic, "Cutting the cord: Static and dynamic inductive wireless charging of electric vehicles," *IEEE Electrific. Mag.*, vol. 1, no. 1, pp. 57–64, Sep. 2013.
- [6] A. Mashinsky, "Self-charging electric vehicles and aircraft, and wireless energy distribution system," U.S. Patent 8890472, Nov. 18, 2015.
- [7] S. Aldhafer, P. D. Mitcheson, J. M. Arteaga, G. Kkelis, and D. C. Yates, "Light-weight wireless power transfer for mid-air charging of drones," in *Proc. 11th Eur. Conf. Antennas Propag. (EUCAP)*, Mar. 2017, pp. 336–340.
- [8] C. H. Choi, H. J. Jang, S. G. Lim, H. C. Lim, S. H. Cho, and I. Gaponov, "Automatic wireless drone charging station creating essential environment for continuous drone operation," in *Proc. Int. Conf. Control, Autom. Inf. Sci. (ICCAIS)*, Oct. 2016, pp. 132–136.
- [9] *Qi*. Accessed: 2019. [Online]. Available: <https://www.wirelesspowerconsortium.com/knowledge-base/magnetic-induction-technology/resonance/qi-wireless-charger-resonant-as-well-as-inductive.html>
- [10] Y. Li, Y. Wang, Y. Cheng, X. Li, and G. Xing, "QiLoc: A Qi wireless charging based system for robust user-initiated indoor location services," in *Proc. 12th Annu. IEEE Int. Conf. Sens., Commun., Netw. (SECON)*, Jun. 2015, pp. 480–488.
- [11] D. R. Smith *et al.*, "An analysis of beamed wireless power transfer in the Fresnel zone using a dynamic, metasurface aperture," *J. Appl. Phys.*, vol. 121, no. 1, Jan. 2017, Art. no. 014901.
- [12] B. S. Mingzhao and P. Kapitanova, "Smart table based on a metasurface for wireless power transfer," *Phys. Rev. Appl.*, vol. 11, no. 5, 2019, Art. no. 054046.

- [13] F. Liu, P. Jayathurathnage, and S. A. Tretyakov, "Active metasurfaces as a platform for capacitive wireless power transfer supporting multiple receivers," in *Proc. 13th Int. Congr. Artif. Mater. Novel Wave Phenomena (Metamater.)*, Sep. 2019, pp. X-227–X-229.
- [14] J. Jadidian and D. Katabi, "Magnetic MIMO: How to charge your phone in your pocket," in *ACM MobiCom*, 2014, pp. 495–506.
- [15] Google. *OpenThread Framework*. Accessed: 2019. [Online]. Available: <https://openthread.io>
- [16] Qi. Accessed: 2019. [Online]. Available: <https://www.wirelesspowerconsortium.com/knowledge-base/magnetic-induction-technology/how-it-works/coupling-factor.html>
- [17] A. Kurs, A. Karalis, R. Moffatt, J. D. Joannopoulos, P. Fisher, and M. Soljacic, "Wireless power transfer via strongly coupled magnetic resonances," *Science*, vol. 317, no. 5834, pp. 83–86, Jul. 2007.
- [18] L. Shi, Z. Kabelac, D. Katabi, and D. Perreault, "Wireless power hotspot that charges all of your devices," in *Proc. 21st Annu. Int. Conf. Mobile Comput. Netw. (MobiCom)*, 2015, pp. 2–13.
- [19] W. Zhong, C. K. Lee, and S. Y. R. Hui, "General analysis on the use of tesla's resonators in domino forms for wireless power transfer," *IEEE Trans. Ind. Electron.*, vol. 60, no. 1, pp. 261–270, Jan. 2013.
- [20] C. K. Lee, W. X. Zhong, and S. Y. R. Hui, "Effects of magnetic coupling of nonadjacent resonators on wireless power domino-resonator systems," *IEEE Trans. Power Electron.*, vol. 27, no. 4, pp. 1905–1916, Apr. 2012.
- [21] C. J. Stevens, "Magnetoinductive waves and wireless power transfer," *IEEE Trans. Power Electron.*, vol. 30, no. 11, pp. 6182–6190, Nov. 2015.
- [22] B. Wang, W. Yerazunis, and K. H. Teo, "Wireless power transfer: Metamaterials and array of coupled resonators," *Proc. IEEE*, vol. 101, no. 6, pp. 1359–1368, Jun. 2013.
- [23] J. Xiong and K. Jamieson, "Arraytrack: A fine-grained indoor location system," in *Proc. Symp. Netw. Syst. Design Implement. (NSDI)*, 2013, pp. 71–84.
- [24] U. Ha, Y. Ma, Z. Zhong, T.-M. Hsu, and F. Adib, "Learning food quality and safety from wireless stickers," in *Proc. 17th ACM Workshop Hot Topics Netw. (HotNets)*, 2018, pp. 106–112.
- [25] J. E. Sundeen and R. C. Buchanan, "Thermal sensor properties of cermet resistor films on silicon substrates," *Sens. Actuators A, Phys.*, vol. 90, nos. 1–2, pp. 118–124, May 2001.
- [26] Y. Zhang, G. Laput, and C. Harrison, "Electrick: Low-cost touch sensing using electric field tomography," in *Proc. CHI Conf. Hum. Factors Comput. Syst.*, 2017, pp. 1–14.
- [27] R. R. A. Syms, L. Solymar, and E. Shamonina, "Absorbing terminations for magneto-inductive waveguides," *IEE Proc., Microw. Antennas Propag.*, vol. 152, no. 2, p. 77, 2005.
- [28] E. Shamonina, V. A. Kalinin, K. H. Ringhofer, and L. Solymar, "Magneto-inductive waveguide," *Electron. Lett.*, vol. 38, no. 8, pp. 371–373, 2002.
- [29] E. Shamonina, V. A. Kalinin, K. H. Ringhofer, and L. Solymar, "Magnetoinductive waves in one, two, and three dimensions," *J. Appl. Phys.*, vol. 92, no. 10, pp. 6252–6261, Nov. 2002.
- [30] S. C. Tang and N. J. McDannold, "Power loss analysis and comparison of segmented and unsegmented energy coupling coils for wireless energy transfer," *IEEE J. Emerg. Sel. Topics Power Electron.*, vol. 3, no. 1, pp. 215–225, Mar. 2015.
- [31] Q. Deng *et al.*, "Frequency-dependent resistance of litz-wire square solenoid coils and quality factor optimization for wireless power transfer," *IEEE Trans. Ind. Electron.*, vol. 63, no. 5, pp. 2825–2837, May 2016.
- [32] J. Craninckx and M. S. J. Steyaert, "A 1.8-GHz low-phase-noise CMOS VCO using optimized hollow spiral inductors," *IEEE J. Solid-State Circuits*, vol. 32, no. 5, pp. 736–744, May 1997.
- [33] E. P. Conversion. (2019). *Class d Amplifier*. [Online]. Available: https://epc-co.com/epc/Portals/0/epc/documents/guides/EPC9512_qsg.pdf
- [34] Y. Cheng and Y. Shu, "A new analytical calculation of the mutual inductance of the coaxial spiral rectangular coils," *IEEE Trans. Magn.*, vol. 50, no. 4, pp. 1–6, Apr. 2014.
- [35] M. K. Kazimierzczuk, "Class D voltage-switching MOSFET power amplifier," *IEE Proc. B Electr. Power Appl.*, vol. 138, no. 6, p. 285, 1991.
- [36] *THREAD*. Accessed: 2019. [Online]. Available: <https://openthread.io/guides/thread-primer>
- [37] K. Li, U. Muncuk, Y. Naderi, and K. Chowdhury, "Softsense: Collaborative surface-based object sensing and tracking using networked coils," in *Proc. GLOBECOM*, Dec. 2019, pp. 1–6.



Kai Li (Student Member, IEEE) received the B.S. degree in applied physics from Qingdao University, China, in 2014, and the M.S. degree in physics from Qingdao University, China, in 2017. He is currently pursuing the Ph.D. degree in electrical engineering with Northeastern University, Boston, MA, USA, in 2017, under the supervision of Prof. K. R. Chowdhury. His research interests include design, optimization and implementation of electromagnetic field in near-field, system design for magnetic resonant coupling-based power transfer, lower power to high power amplifier circuit design, analog and digital circuit design, as well as wireless mesh networks. He was a recipient of Best Paper Awards at the IEEE GLOBECOM in 2019.



Ufuk Muncuk (Student Member, IEEE) received the Ph.D. degree in electrical and computer engineering from Northeastern University, Boston, MA, USA, in 2019. He is currently a Post-Doctoral Research Associate at the Electrical and Computer Engineering Department, Northeastern University. His research interests include design, optimization, and implementation for RF energy harvesting circuits, use of wireless energy transfer, system design for joint RF energy and magnetic coupling-based energy transfer, system design for intra-body transceivers, analog and digital circuit design, wireless sensor networks, and cognitive radio systems. He was a recipient of the Best Paper Runners-up at ACM SenSys 2018, as well as the Best Paper Awards at the IEEE ICC in 2013 and the IEEE GLOBECOM in 2019.



M. Yousof Naderi (Member, IEEE) received the Ph.D. degree from Northeastern University, Boston, in December 2015. He is a Principal Research Scientist with the Department of Electrical and Computer Engineering, Northeastern University, and an Associate Member of the Institute for the Wireless Internet of Things. His expertise and research interests lie in AI-powered cyber-physical systems, next-generation wireless charging solutions, and software-defined networks. On these areas, he has coauthored numerous publications and served as a chair, a TPC member, and a reviewer of many conferences and journals, including an Organizing Member of the New England Workshop on Software Defined Radio (NEWSDR) from 2017 to 2020. He is also serving as an Organizing Member of the NEWSDR. He was a recipient of the NEU Ph.D. Dissertation Award in 2015 and best paper awards from INFOCOM 2018 and the IEEE GLOBECOM 2019.



Kaushik Roy Chowdhury (Senior Member, IEEE) received the M.S. degree from the University of Cincinnati in 2006, and the Ph.D. degree from the Georgia Institute of Technology in 2009. He was an Assistant Professor at Northeastern University from 2009 to 2015, where he is currently an Associate Professor with the Electrical and Computer Engineering Department. His current research interests include dynamic spectrum access, wireless RF energy harvesting, and the IoT and in the area of intra/on-body communication. He was a winner of the Presidential Early Career Award for Scientists and Engineers (PECASE) in 2017, the ONR Director of Research Early Career Award in 2016, and the NSF CAREER Award in 2015.